Horizontally homogeneous rotating radiative-convective equilibria at GCM resolution

Isaac M. Held
Geophysical Fluid Dynamics Laboratory / NOAA Princeton, New Jersey

Ming Zhao
Program in Atmospheric and Oceanic Sciences, Department of Geosciences, Princeton University, Princeton, New Jersey

Revised, Journal of the Atmospheric Sciences

Corresponding author address:

Dr. Isaac M. Held,

Geophysical Fluid Dynamics Laboratory / NOAA

Princeton University Forrestal Campus / US Route 1

P.O.Box 308 Princeton

New Jersey 08542

Abstract.

Rotating radiative-convective equilibrium, using the column physics and resolution of GCMs, is proposed as a useful framework for studying the tropical storm-like vortices produced by global models. We illustrate these equilibria using the column physics and dynamics of a version of the GFDL AM2 model at resolutions of 220, 110, and 55 km, in a large 2×10^4 km square horizontally homogeneous domain with fixed sea surface temperature and uniform Coriolis parameter. The large domain allows a number of tropical storms to exist simultaneously. Once equilibrium is attained, storms often persist for hundreds of days. The number of storms decreases as sea surface temperatures increase, while the average intensity increases. As the background rotation is decreased, the number of storms also decreases. At these resolutions and with this parameterization of convection, a dense collection of tropical storms is always the end state of moist convection in the cases examined.

1. Introduction

The tropical storms or storm-like vortices that develop in global models have been studied for clues as to the response of these storms to global warming (e.g., Broccoli and Manabe 1990; Bengtsson et al. 1995 1996; Sugi et al. 2002; McDonald et al. 2005; Chauvin et al. 2006; Yoshimura et al. 2006). Global atmospheric model simulations, using as boundary conditions the sea surface temperature (SST) from coupled climate models, are useful as a first approach to this problem, and these are now typically conducted at 50-100 km resolution, while 20 km resolution simulations are feasible (Oouchi et al. 2006). It is reasonable to expect that our understanding of the sensitivity of the climatology of tropical cyclones to warming will advance as work with high resolution global models continues to progress. We propose a framework here that we hope will be of value in analyzing the tropical storm-like vortices in GCMs.

Held et al. (2007) (hereafter HZW) describe the radiative-convective equilibria of a model in which the column physics of a GCM is coupled to non-rotating hydrostatic dynamics in a periodic box, assuming horizontally homogeneous SSTs. HZW argue that this is a useful geometry in which to study some of the consequences of the choice of column physics for tropical convection and cloud feedbacks in the global model. While higher resolution simulations of radiative-convective equilibrium are available, HZW intentionally use resolutions that are close to those of the parent GCMs whose behavior they hope to clarify with these more idealized models. They do find some similarities between the response of the tropics to increasing SSTs in the full GCM and in the homogeneous non-rotating model.

In this paper, we describe a rotating version of this non-cloud-resolving model of radiative-convective equilibrium. Nolan et al. (2007) describe a similar framework but with much higher "cloud-resolving" resolution. Bretherton et al. (2005) also briefly describe a high resolution example of rotating radiative-convective equilibrium. In both of these cases, the domain is sufficiently small that only one tropical storm develops within the model. We consider domains large enough that multiple storms can co-exist, with resolutions ranging from 50 to 200 kms, resolutions directly relevant to global models that are under study at our institution and elsewhere.

We do not claim that models of this resolution provide fully convincing simulations of rotating radiative-convective equilibrium. More definitive simulations in these large domains will require a much larger expenditure of computational resources. Our hope, in the meantime, is that models of this type will be valuable in relating high resolution cloud-resolving models to the models in use for studies of global warming, and in trying to understand the differences between the responses to warming in the tropical cyclone-like vortices in different global models.

2. Model Formulation and control simulations

As in HZW, we remove spherical geometry from a version of the global model, GFDL's AM2p12b described in Anderson et al. (2004), and introduce doubly periodic boundary conditions, but set the Coriolis parameter to its value at 10N. The column physics package and vertical level spacing are unmodified from that in the global model. Of the 24 model levels, 10 are in the lowest 2 km, with the lowest model level at $\sim$35 meters; we refer the reader to Anderson et al. (2004) for further details. Also as in HZW, there is no diurnal and no seasonal cycle, while the stratospheric water vapor is initialized with realistic values but cannot equilibrate on the time scale of the calculations performed. (Indeed, in this configuration, stratospheric water equilibrates much more slowly than in more realistic models, due to the absence of a Brewer-Dobson circulation.) SSTs are prescribed and horizontally homogeneous. We use a domain with 90x90 gridpoints for the model with 220 km resolution, and retain the same size physical domain as we decrease the grid to 110 and 55 kms. The choice of such a large domain is motivated by the desire to avoid finite-size effects, particularly the situation of a single storm interacting with images of itself through the periodic boundary conditions, and to leave room for the simultaneous existence of multiple storms. We integrate the model for 360 days, discarding the first 90 days as spin-up. A 90-day spin-up was judged adequate based on examination of the domain averaged thermodynamic profile as well as storm statistics. The length of the averaging period was determined by trial and error with the goal of obtaining consistent variations in storm statistics for the parameter variations described in the following. The trend in lower stratospheric

water vapor over this time period is very small (-6%) and we see no significant trends at or below the tropopause.

In all of our simulations with this 10N setting of the Coriolis parameter, the final state of the model consists of a set of rotating storms that appear to be as closely packed as allowed by the storm structure, as illustrated in Fig. 1 for each of the three horizontal resolutions employed. The storms persist for very long times, with an occasional collapse often followed by redevelopment to maintain roughly the same spacing between storms. In many cases, individual storms, once formed, persist for most of the length of the integration. The number of storms increases with finer resolution, although there is a suggestion of convergence as one moves from 110 to 55 km resolution. The 220 km model is the outlier among these three configurations in most statistics examined.

The precipitation that falls near the storm center is invariably dominated by grid-scale condensation, while rainfall associated with the convective parameterization dominates as one moves away from the storm. Therefore, the ratio of large-scale to convective rainfall is a useful measure of how much of the domain-averaged rain is associated with the storm centers. This ratio is approximately 40% in the 55 km and 110 km simulations with 301K SSTs and is lower (25%) in the 220 km version. The rainfall in the model rain bands is typically generated by the convective closure, so the total storm-associated rainfall is larger than this value, but difficult to quantify in a way that is not dependent on an arbitrary definition of storm size. However, casual inspection of the figure suggests that most of the rainfall in this model is, in fact, associated with storms.

Crude eye formations appear, especially at the 55 km resolution, at times with a relatively well-defined radius of maximum winds, as seen in Figure 1, but these are too close to the grid scale to warrant study of the size of the eye as a function of model parameters. Also evident from the figure are the well-defined surface pressure minima that allow a fairly simple storm counting algorithm. In the following, we count storms by identifying patches of surface pressure below 1000 hPa (the mean pressure is 1005.5 hPa). There is little sensitivity to this pressure criterion, as almost all storms sustains surface pressures well below this value. Unlike storm counting

algorithms in more realistic models, there is no need to test for warm core structure to distinguish between tropical and extratropical cyclones.

3. Sensitivity to SST

We obtain statistical equilibria for SSTs between 297 K and 305 K at a 2 K interval. Snapshots of the precipitation for SSTs of 297 K and 305 K are compared in Fig 2. The numbers of storms for different resolutions and SSTs are shown in Fig 3. The number of storms decreases with increasing SST at all three resolutions. Once statistically steady states are attained, the instantaneous number of storms typically remains within 1 or 2 of that shown in Fig 3.

We compute the minimum surface pressure in each identified storm from 3-hourly instantaneous output and then generate a frequency distribution of these intensities. The results are shown in Fig 4, as are similarly constructed PDFs for maximum surface wind speed. (The "surface wind" here is the wind in the lowest model layer, at roughly 35 meters.). The decrease in minimum surface pressure and increase in maximum wind with increasing temperature are evident at all resolutions, but these variations are particularly consistent and smooth in the 55 km model.

The storms in this model have relatively weak maximum winds for a given surface pressure as compared to observations, implying that the typical storm is of too large a size at these low resolutions. The storms at the peak in the PDF in the 55 km model, with a central pressure of 965 hPa, have maximum winds of about 35 ms^{-1}. In contrast, the average observed Atlantic storm with this central pressure has winds of 50 ms^{-1} (Landsea 1993).

The close-packed nature of the storms in these simulations encourages the identification of the average storm spacing with an outer storm radius. One can speculate that a tendency towards a self-similar structure might favor a particular ratio between the outer radius and the radius of maximum winds. This would provide a possible rationalization of the larger outer radius in the lowest resolution simulations, in which the inner radius is large and diffuse. However, the number of storms is only slightly larger at 55 than at 110 km resolution, and one might expect the grid size

to be limiting the inner radius of storms at these resolutions as well.

We compute the minimum surface pressure and maximum surface wind within the entire domain at each instant of time and then average over time to obtain the plots in Fig 5. Also displayed in the lower panels are the global extrema attained at any time or location in each integration, as well as estimates of the maximum potential intensity (MPI). The latter are obtained following Emanuel (1999), utilizing the code provided at `http://wind.mit.edu/~emanuel/home.html` and the domain-averaged thermodynamic profiles from the 55km simulations. We choose the options of pseudo-adiabatic ascent and the inclusion of dissipative heating as most relevant to our simulations. The ratio of the surface drag coefficient for heat and vapor (C_k) to that for momentum exchange (C_d) is a key parameter in the theory. Using the drag formulation from the AM2 GCM, taken from Beljaars (1995), this ratio decreases as wind speeds approach hurricane strength, with values of 0.6 typical beneath the model's strongest winds. In the figure, we display results for both C_k/C_d = 0.6 and 0.8. These small values are not thought to be realistic, and they evidently play some role in limiting the strength of the model's storms.

A consistent picture of intensification is evident as SST increases. One also sees some intensification with increasing resolution. The sensitivity to SST here is a bit less than 2 hPa intensification for a 1 K increase in SST for the typical storm, from Fig 4, and at most about 3 $\mathrm{hPa\,K^{-1}}$ for the most intense storms in the integrations, from Fig 5, corresponding an increase in the pressure drop between the storm center and the domain mean of about 4-6% $\mathrm{K^{-1}}$. These sensitivities are comparable to the median changes quoted by Knutson et al. (1998) as obtained at much higher resolution with the GFDL Hurricane Prediction System. Maximum wind speeds increase at roughly 1.5-2% $\mathrm{K^{-1}}$ for the most intense storms in the 55 km model. The expectation for a balanced vortex with no change in storm size is that the fractional pressure drop be double the fractional increase in the wind speed, so these results are consistent with an increase in storm size associated with an increase in the spacing between storms as SSTs warm.

The estimated MPI increases with warming SSTs at roughly the same rate as does the peak

intensities in the model. We have performed preliminary calculations which show that this model does create stronger storms if the drag coefficients are modified to create a larger C_k/C_d ratio under strong winds. Initial indications are that the effect is weaker than that predicted by the MPI theory, suggesting that cyclone strength is limited by resolution as well, but we defer closer analysis of this question.

The surface wind stress multiplied by the surface wind speed, approximately proportional to the kinetic energy dissipated in the surface boundary layer, increases with temperature at the rate of $\sim 3\% \ \mathrm{K}^{-1}$ when averaged over the domain. The precipitation in the domain also increases with SST, at about the same rate. Therefore the energy dissipation near the surface per unit precipitation stays unchanged, to first approximation, as illustrated in Fig 6. The domain-averaged precipitation, or evaporation, is a measure of the energy source at the surface, or equivalently the energy sink due to net radiative cooling (longwave cooling plus shortwave heating) in the free troposphere. The constancy of energy dissipation normalized by the precipitation suggests that the thermodynamic efficiency, the generation of kinetic energy per unit energy source, stays roughly constant as the SSTs increase.

Whereas the domain averaged wind speed cubed increases at $\approx 3\% \ \mathrm{K}^{-1}$, the maximum wind speed cubed in the most intense storms increases at $\approx 8\% \ \mathrm{K}^{-1}$, corresponding to an increase in the maximum wind speed itself of $\approx 1.5 - 2\% \ \mathrm{K}^{-1}$ (Fig 5). The wind speed increase in the typical storm is smaller than the increase in the most intense storms.

The cloud radiative forcing in this rotating model is not sensitive to SST, staying close to -40 $\mathrm{W\,m^{-2}}$ in all of the simulations at 110 km and 55 km resolutions. This insensitivity contrasts with the results of the non-rotating case described in HZW, where changes in convective organization result in large changes in the cloud forcing as a function of SST. In the presence of rotation, the convective organization into a set of closely-packed vortices is robust, and the changes in the radiative fluxes are more modest as a result.

In the non-rotating case, HZW show that one can predict the cloud radiative forcing in this model if one is given f_ℓ, the fraction of the precipitation that is large-scale rather than convective

(that is, produced by the model's convection parameterization). This is the case even though both f_ℓ and the cloud forcing vary substantially as the resolution and the entrainment rate in the plumes underlying the convection scheme are varied. Interestingly, these rotating experiments fall on the same functional relationship between f_ℓ and cloud forcing; if one creates a non-rotating case with the same value of f_ℓ as in this rotating case (40%), it has about the same cloud forcing as the rotating case as well ,-40 $\mathrm{W\,m^{-2}}$, as seen in Figure 5 of HZW.

Relative humidities (not shown) change hardly at all, so vapor increases at the Clausius-Clapeyron (C-C) rate of roughly 6% $\mathrm{K^{-1}}$. Precipitation increases less rapidly, as we have seen, presumably because it is constrained by the energy balance of the troposphere (e.g., Betts 1990; Knutson and Manabe 1995; Held and Soden 2000). If the number and structure of the storms do not change, then one might expect the storm precipitation to increase at the C-C rate, contrary to the model result. This provides one possible line of argument for why there are fewer storms as SSTs increase. A key to this argument is the assumption that the storms account for a large percentage of the precipitation. In the atmosphere, the fraction of tropical precipitation that falls in tropical cyclones is small; so this kind of argument cannot be used to directly constrain the storm number in nature. The fraction of precipitation in the storms could simply increase.

An alternative explanation for the reduction in number of storms with increasing SST in this geometry is suggested by experiments in which the rotation rate is changed.

4. Varying the rotation rate

To help in thinking about the controls on the number and spacing of storms, we have conducted several experiments with altered rotation rates. Fig 7 illustrates the results obtained at 55 km resolution with SST = 305 K, with Coriolis parameter set at the 5N and 20N values, rather than the 10N value utilized above. Results at other values of SST are similar. The number of storms generated at 5, 10, and 20N rotation rates are summarized in Fig 8 for the 110 and 55 km models. The smaller number of storms in the 220 km model, especially at the smallest rotation rate, makes it less useful for this purpose.

Eye walls are relatively well defined at the 5N rotation rate and the 55 km resolution, as seen in Fig 7. There is a well-defined increase in eye radius with increasing height (not shown). The radius of eye increases along with the storm spacing as rotation is reduced. Some of these eyes have diameters approaching 1,000 kms with the 5N setting.

The 110 km and 55 km models produce about the same number of storms at the 5N and 10N rotation rates, but the higher resolution model produces 50% more storms for the 20N setting, as seen in Fig 8. Given the small size of the storms in this case, this lack of convergence is not surprising. If one focuses on the 5N and 10N settings, and the finest resolution model, the increase in number of storms is faster than linear in f, but slower than quadratic. But the suggestion from the 55 km-110 km comparison is that a still finer resolution would generate more storms at the 10N setting, potentially resulting in a stronger dependence on rotation.

Since we are counting storms in a two-dimensional region, if the spacing between storms were inversely proportional to f, the number would be proportional to f^2. The dry radius of deformation provides an example of a scale with this property. Scaling of the storm scale with the radius of deformation also provides an alternative explanation for the decrease in storm number with increasing SST. The dry stability, N^2, average over the troposphere must increase with SST at roughly the C-C rate, in order that the profile remain close to a moist adiabatic. The result is an increase in N, and the radius of deformation, of roughly 3% per degree warming.

However, it is not self-evident that the Rossby radius controls the spacing between these tropical storms. An alternative is provided by the scale $\mathcal{L} \equiv V_m/f$ (Emanuel 1988), where V_m is the maximum potential intensity, a function of the environmental thermodynamic profile and surface exchange coefficients. If one assumes that the average storm's maximum winds scale with V_m, and that the ratio of the radius of maximum winds (r_m) to the outer radius of the storm (r_o), at which the flow is dominated by the ambient rotation, is fixed, then the outer radius, r_o, will scale with L. That is, conserving angular momentum,

$$\frac{f}{2}r_o^2 = \frac{f}{2}r_m^2 + V_m r_m \tag{1}$$

or, setting $\xi \equiv r_m/r_o$,

$$r_o = 2\mathcal{L}\frac{\xi}{1-\xi^2} \tag{2}$$

To the extent that the storms are close packed, we might then expect that the spacing scales with $\mathcal{L}$, and the number of storms with f^2.

The scale $\mathcal{L} = V_m/f$ also provides a possible explanation for the reduction in the number of storms with increasing SST, since storm intensity increases as SST increases. If we take as relevant the actual maximum winds, which increase by roughly 1.5-2% K^{-1}, this translates into a 3-4% K^{-1} decrease in number, or about 25-30% for the 8 K change shown in Fig 3, roughly consistent with the model's decrease in number displayed in that figure.

In contrast to the changes in scale, the changes in intensity as the rotation rate is varied are relatively small, as seen in Fig 8, consistent with the view that intensity is primarily controlled by the thermodynamics.

Given that the flow is still dominated by (very large) tropical storms at the lowest rotation rate examined, it appears that the $f \to 0$ limit is rather singular in large domains, with the transition to the non-rotating morphology occurring only when storms grow so large that they can no longer fit into the domain. However, one suspects that the storms that form at low rotation rates are relatively fragile in the presence of environmental shear. Both Jones (1995) and Reasor et al. (2004) point out that larger vortices are more stable to distortion by vertical shear, for fixed radius of deformation, because vertical coupling increases in strength with horizontal scale. But here the radius of deformation is increasing along with the cyclone scale, so this stabilizing effect is neutralized. Because intensity is approximately unchanged as the storms expand with decreasing ambient rotation in this model, the vorticity of the storms decreases. We suspect that this reduction in vorticity makes it easier for large-scale shears, especially horizontal shears, to destroy these vortices.

5. Conclusions

There is a need for simplified versions of atmospheric climate models that help us connect theory with comprehensive modeling efforts. Thinking of a model as built from a dynamical core and column physics, one can, in particular, either retain the dynamical framework and simplify the physics or simplify the dynamical framework and retain the column physics. Here we take the latter path along the lines of Held et al. (2007) (HZW), replacing the inhomogeneous spherical problem with a homogeneous doubly periodic radiative-convective framework. The non-rotating case discussed by HZW is here generalized to an f-plane geometry.

The change in convective organization due to rotation is profound, with the flow dominated by closely packed tropical storms, at least with the column physics package utilized here. The result is a distinctive kind of turbulence, dominated by vortices, but differing in many fundamental respects from the more familiar vortex-dominated two-dimensional flows. The flow here is strongly dissipative, and the vortices survive only as long as they successfully compete for the available evaporation.

We have examined some of the statistical properties of this rotating convective turbulence dominated by tropical storms by varying model resolution, sea surface temperatures, and rotation rate. The resolution studies hint at convergence in storm number and size in the range of 50-100 km, for a 10N Coriolis parameter at least, a range of resolutions that is increasingly being populated by atmospheric models utilized in climate change studies. But this result may be sensitive to the convective parameterization, and calculations at much higher resolution would be needed to provide more convincing evidence of this convergence.

When SSTs are increased, the average intensity of the storms increases and the number decreases. These two effects may be related, if the storm scale and spacing are controlled by the horizontal scale V_m/f, where V_m is the strength of the maximum winds. When rotation rates are increased, the size of the average storm clearly decreases, and the number increases, also more or less as expected from this scaling. Alternatively, scaling storm spacing with the radius of deformation could also simultaneously explain the rotation rate and SST dependence obtained

in this model, since the dry static stability increases with SST. We also feel that the fact that the thermodynamic efficiency of the model changes hardly at all as SSTs are changed is important for theories of these statistically steady states. We do not attempt to choose between these alternative approaches here.

The relevance of these homogeneous results to realistic inhomogeneous environments, in nature or, for that matter, in comprehensive models, is not straightforward. The distinctive property of these equilibria is that storms are generated till they reach some natural close-packed configuration, after which storm generation and decay are rare. To create more realistic flows, a loss mechanism is required. Given an efficient loss mechanism, the number of storms will then depend on the rate of generation and not simply on the preferred close-packed configuration. How best to include a loss mechanism to replace realistic migration over land or into highly sheared mid-latitude environments while retaining a homogeneous model is unclear. It is likely that simple inhomogeneous configurations will be needed for this purpose. One can also add shear so as to interfere with the storm generation process itself. In a large f-plane geometry, extra complications arise with the addition of shear, besides those related to the interaction between shear and storm genesis, in that a balanced shear introduces the potential for baroclinic instability and competition between stabilization by moist convection and by baroclinic eddies.

In addition to increasing the realism of the model, it should, alternatively, also be of interest to simplify the physics in the homogeneous rotating setting, so as to isolate the controls on storm size and structure more cleanly.

Finally, it would also be of interest to compare simulations of this type with identical column physics but different algorithms for the fluid dynamical core, to see if these results are sensitive to the choice of discretization.

Acknowledgments The authors thank Steve Garner and S.-J. Lin for helpful comments on this paper, and Kerry Emanuel and David Nolan for discussion of the horizontal scale of tropical

storms. We also thank Bruce Wyman for his work in configuring the doubly-periodic model. Ming Zhao was supported in part by NSF Grant ATM-0612551 and in part under award NA17RJ2612 from the National Oceanic and Atmospheric Administration, U.S. Department of Commerce. The findings are those of the authors and do not necessarily reflect the views of the National Oceanic and Atmospheric Administration, or the U.S. Department of Commerce.

References

Anderson, J., V. Balaji, A. Broccoli, W. Cooke, T. Delworth, K. Dixon, L. Donner, K. Dunne, S. Freidenreich, S. Garner, R. Gudgel, C. Gordon, I. Held, R. Hemler, L. Horowitz, S. Klein, T. Knutson, P. Kushner, A. Langenhost, N.-C. Lau, Z. Liang, S. Malyshev, M. Nath, J. Ploshay, V. Ramaswamy, M. Schwarzkopf, E. Shevliakova, J. Sirutis, B. Soden, W. Stern, L. Thompson, McLean, R. Wilson, A. Wittenberg and B. Wyman, 2004: The new GFDL global atmosphere and land model AM2/LM2: Evaluation with prescribed SST simulations. *J. Climate*, **17**, 4641–4673.

Beljaars, A. C. M., 1995: The parameterization of surface-fluxes in large-scale models under free convection. *Q. J. R. Meteorol. Soc.*, **121**, 255–270.

Bengtsson, L., M. Botzet and M. Esch, 1995: Hurricane-type vortices in a general circulation model. *Tellus*, **47A**, 175–196.

Bengtsson, L., M. Botzet and M. Esch, 1996: Will greenhouse gas-induced warming over the next 50 years lead to higher frequency and greater intensity of hurricanes? *Tellus*, **48A**, 57–73.

Betts, A. K., 1990: Greenhouse warming and the tropical water budget. *Bulletin American Meteorological Society*, **71**, 1464–1465.

Bretherton, C. S., P. N. Blossey and M. Khairoutdinov, 2005: An energy-balance analysis of deep convective self-aggregation above uniform SST. *J. Atmos. Sci.*, **62**, 4273–4292.

Broccoli, A. and S. Manabe, 1990: Can existing climate models be used to study anthropogenic changes in tropical cyclone climate. *Geophys. Res. Let.*, **17**, 1917–1920.

Chauvin, F., J.-F. Royer and M. Deque, 2006: Response of hurricane-type vortices to global warming as simulated by arpege-climat at high resolution. *Clim. Dyn.*, **27**, 377–399.

Emanuel, K. A., 1988: The maximum intensity of hurricanes. *J. Atmos. Sci.*, **45**, 1143–1155.

Emanuel, K. A., 1999: Thermodynamic control of hurricane intensity. *Nature*, **401**, 665–669.

Held, I. M. and B. J. Soden, 2000: Water vapor feedback and global warming. *Annu. Rev. Energy Environ*, **25**, 441–475.

Held, I. M., M. Zhao and B. Wyman, 2007: Dynamic radiative-convective equilibria using GCM column physics. *J. Atmos. Sci.*, **50**, 3909–3927.

Jones, S. C., 1995: The evolution of vortices in vertical shear. I: Initially barotropic vortices. **121**, 821–851.

Knutson, T. K. and S. Manabe, 1995: Time-mean response over the tropical pacific to increased CO2 in a coupled ocean-atmosphere model. *J. Climate*, **8**, 2181–2199.

Knutson, T. K., R. E. Tuleya and Y. Kurihara, 1998: Simulated increase of hurricane intensities in a CO2-warmed climate. *Science*, **279**, 1018–1020.

Landsea, C. W., 1993: A climatology of intense (or major) Atlantic hurricanes. *Mon. Wea. Rev.*, **121**, 1703–1713.

McDonald, R. E., D. G. Bleaken, D. R. Creswell, V. D. Pope and C. A. Senior, 2005: Tropical storms: representation and diagnosis in climate models and the impact of climate change. *Clim. Dyn.*, **25**, 19–36.

Nolan, D. S., E. D. Rappin and K. A. Emanuel, 2007: Could hurricanes form from random convection in a warmer world? *Preprints, 27th AMS Meeting on Hurricanes and Tropical Meteorology, Monterey, CA.*

Oouchi, K., J. Yoshimura, H. Yoshimura, R. Mizuta, S. Kusunoki and A. Noda, 2006: Tropical cyclone climatology in a global-warming climate as simulated in a 20 km mesh global atmospheric model: Frequency and wind intensity analysis. *J. Meteor. Soc. Japan*, **84**, 259–276.

Reasor, P. D., M. T. Montgomery and L. D. Grasso, 2004: A new look at the problem of tropical cyclones in vertical shear flow: Vortex resiliency. *J. Atmos. Sci.*, **61**, 3–22.

Sugi, M., A. Noda and N. Sato, 2002: Influence of the global warming on tropical cyclone

climatology: An experiment with the JMA global model. *J. Meteor. Soc. Japan*, **80**, 249–272.

Yoshimura, J., M. Sugi and A. Noda, 2006: Influence of greenhouse warming on tropical cyclone frequency. *J. Meteor. Soc. Japan*, **84**, 405–428.

Received _____

This manuscript was prepared with AGU's LaTeX macros v4, with the extension package 'AGU^{++}' by P. W. Daly, version 1.6b from 1999/08/19.

Figure captions

Figure 1: Snapshots of precipitation (left, $\mathrm{mm\,day^{-1}}$), surface pressure (middle, hPa) and surface wind speed (right, $\mathrm{m\,s^{-1}}$). Top: 220 km resolution, middle: 110 km resolution, bottom: 55 km resolution. Axes label unit: 1000 km.

Figure 2: Snapshots of precipitation ($\mathrm{mm\,day^{-1}}$) for 55 km resolution and different sea surface temperatures. Left: SST=297 K, right: SST=305 K.

Figure 3: Average number of tropical cyclones within simulation domain.

Figure 4: PDFs of minimum central surface pressure (left column) and maximum surface wind (right column), for 3 different horizontal resolutions (upper: 220 km, middle: 110 km, bottom: 55 km) and 5 different surface temperatures (legend).

Figure 5: Upper panels: time-averaged minimum surface pressure (left) and maximum surface wind speed (right) in the domain. Lower panels: global minimum surface pressure (left) and maximum surface wind speed (right) at any time and location in each integration. Thick lines in the lower panels show the predictions from the MPI theory of Emanuel (1999) with two different values of C_k/C_d.

Figure 6: Domain-averaged surface precipitation rate P, surface kinetic energy dissipation rate $D = \rho C_d U^3$ and the ratio D/P as a function of SST. U is surface (35 m) wind speed, C_d is drag coefficient, ρ is air density. Each of these quantities is divided by its control value at 301 K so as to display the fractional changes.

Figure 7: Snapshots of surface wind speed ($\mathrm{m\,s^{-1}}$) for ambient rotation rates corresponding to 5N (left) and 20N (right), in 55 km model with SST = 305K.

Figure 8: a) Sensitivity of storm number to ambient rotation rate. b) PDF of minimum storm surface pressure as a function of ambient rotation for the 55 km model. c) As in b) but for maximum storm surface wind.

Figure Captions

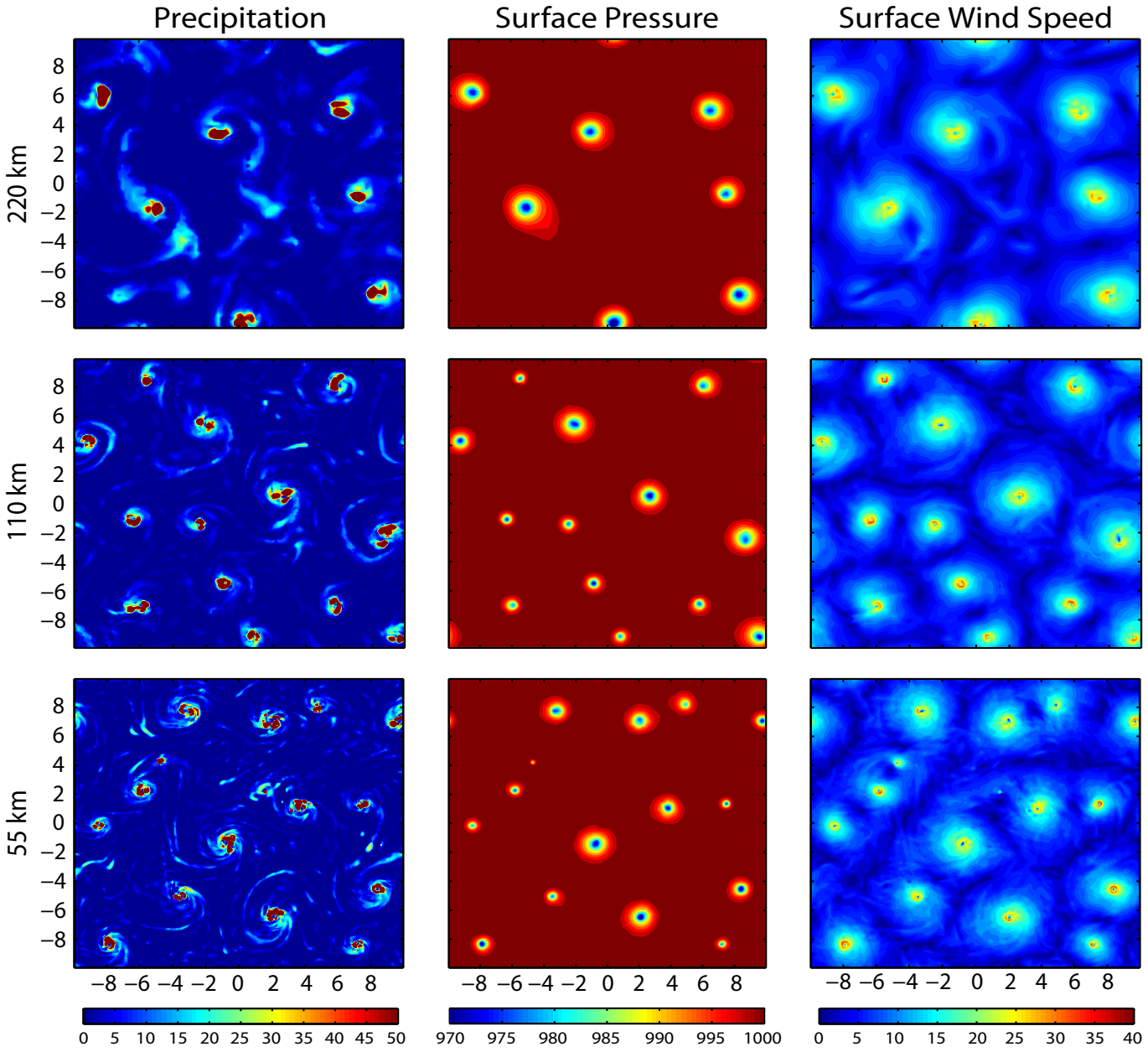

Figure 1. Snapshots of precipitation (left, $\mathrm{mm\,day^{-1}}$), surface pressure (middle, hPa) and surface wind speed (right, $\mathrm{m\,s^{-1}}$). Top: 220 km resolution, middle: 110 km resolution, bottom: 55 km resolution. Axes label unit: 1000 km.

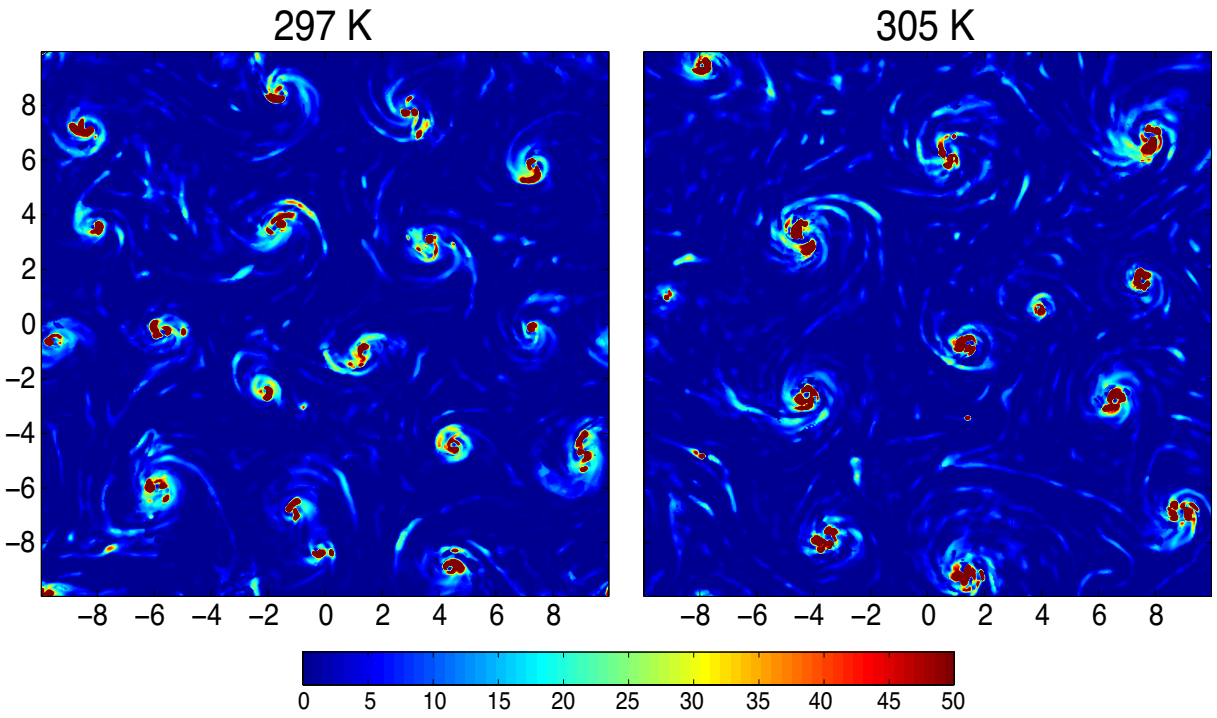

Figure 2. Snapshots of precipitation ($\mathrm{mm\ day^{-1}}$) for 55 km resolution and different sea surface temperatures. Left: SST=297 K, right: SST=305 K.

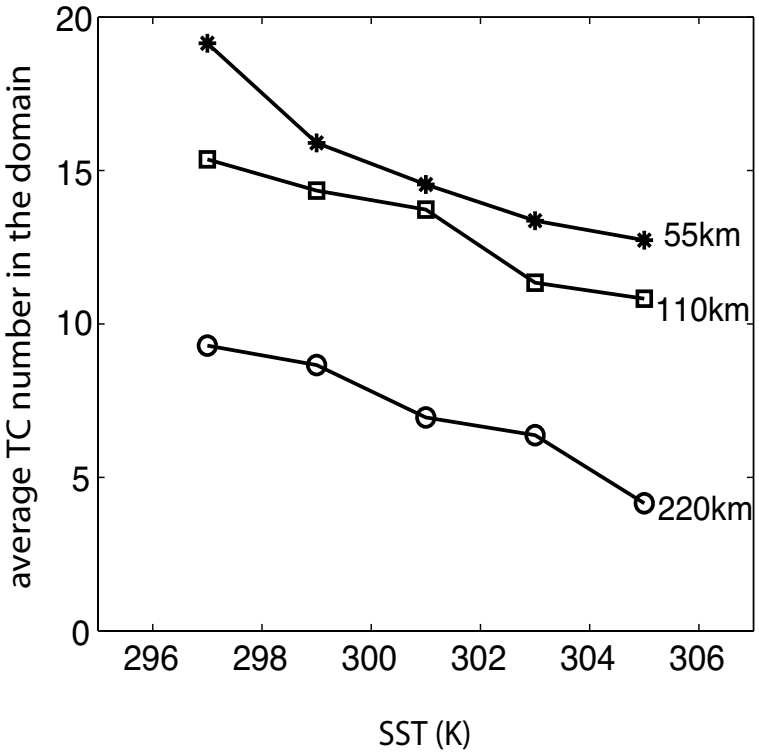

Figure 3. Average number of tropical cyclones within simulation domain.

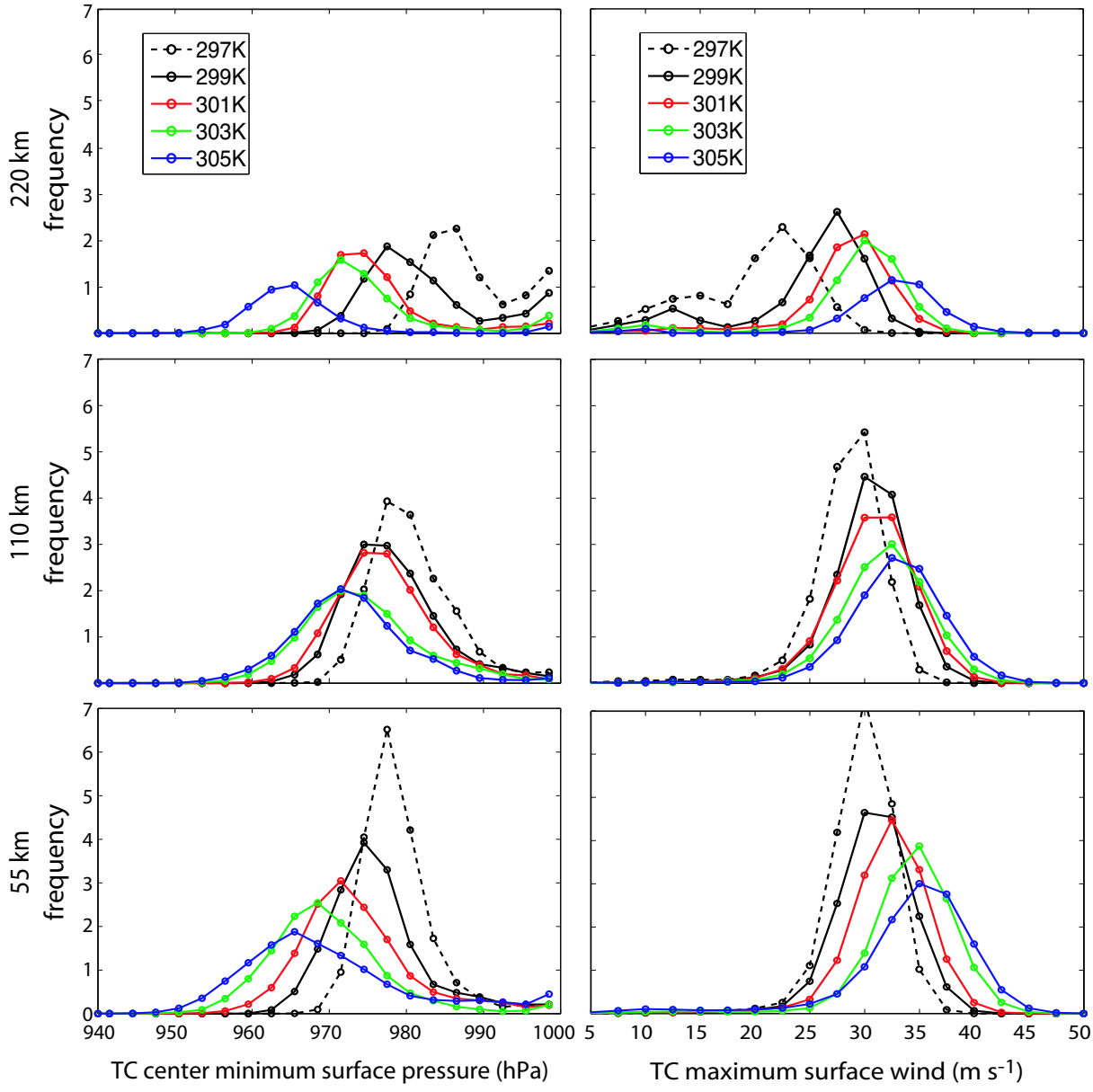

Figure 4. PDFs of minimum central surface pressure (left column) and maximum surface wind (right column), for 3 different horizontal resolutions (upper: 220 km, middle: 110 km, bottom: 55 km) and 5 different surface temperatures (legend).

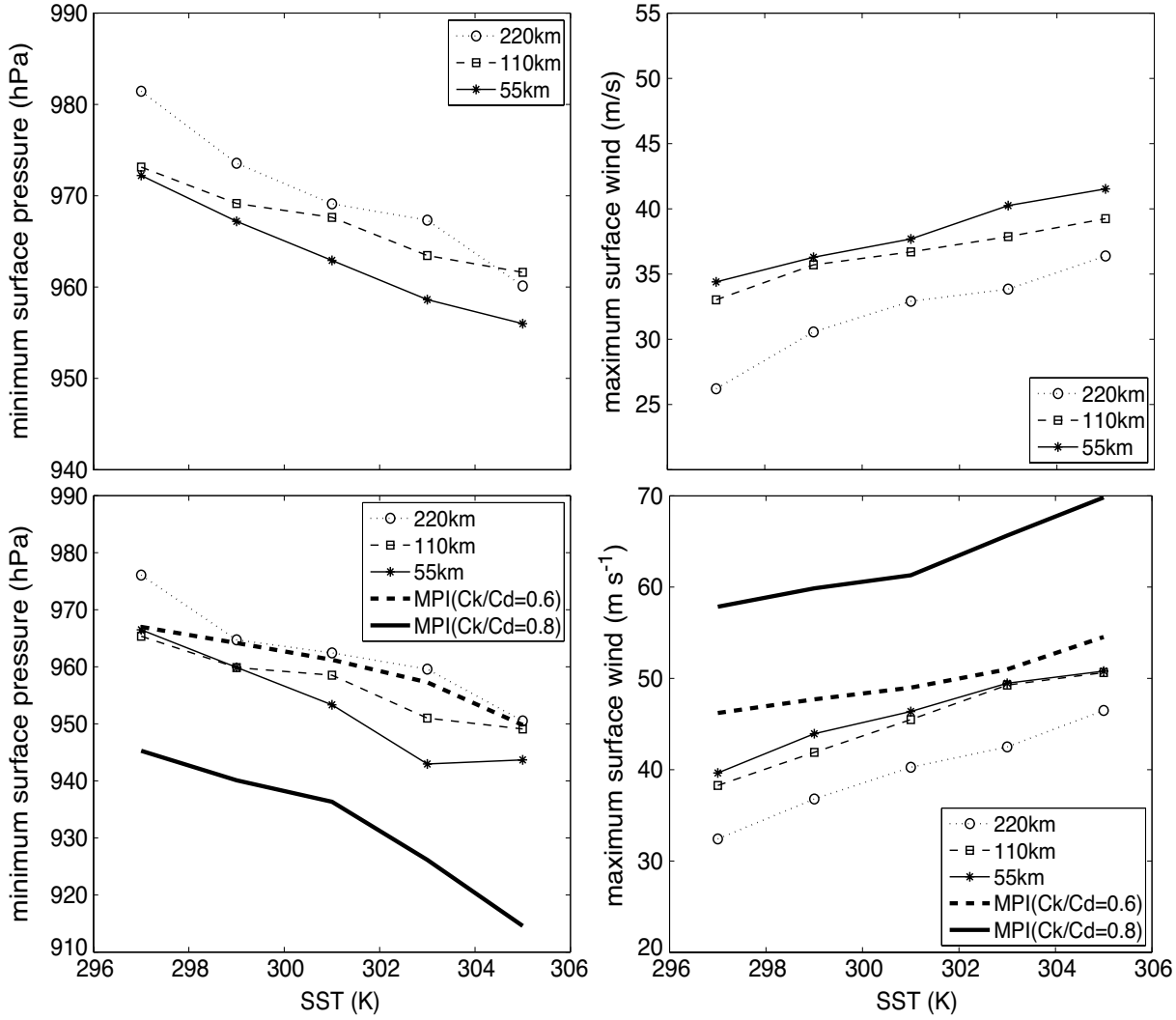

Figure 5. Upper panels: time-averaged minimum surface pressure (left) and maximum surface wind speed (right) in the domain. Lower panels: global minimum surface pressure (left) and maximum surface wind speed (right) at any time and location in each integration. Thick lines in the lower panels show the predictions from the MPI theory of Emanuel (1999) with two different values of C_k/C_d.

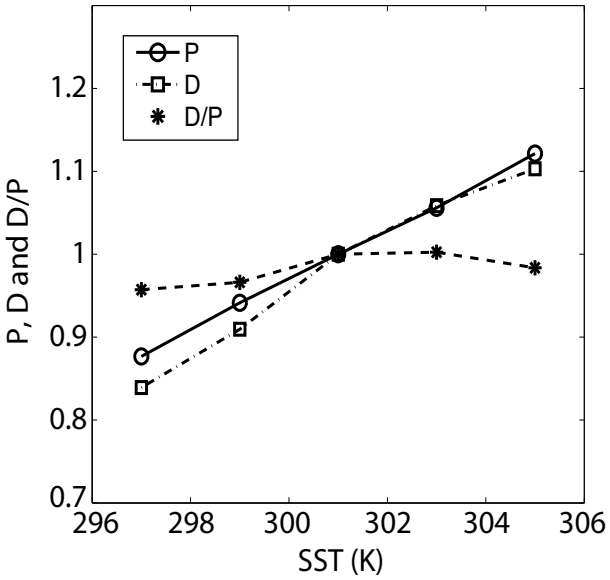

Figure 6. Domain-averaged surface precipitation rate P, surface kinetic energy dissipation rate $D = \rho C_d U^3$ and the ratio D/P as a function of SST. U is surface (35 m) wind speed, C_d is drag coefficient, ρ is air density. Each of these quantities is divided by its control value at 301 K so as to display the fractional changes.

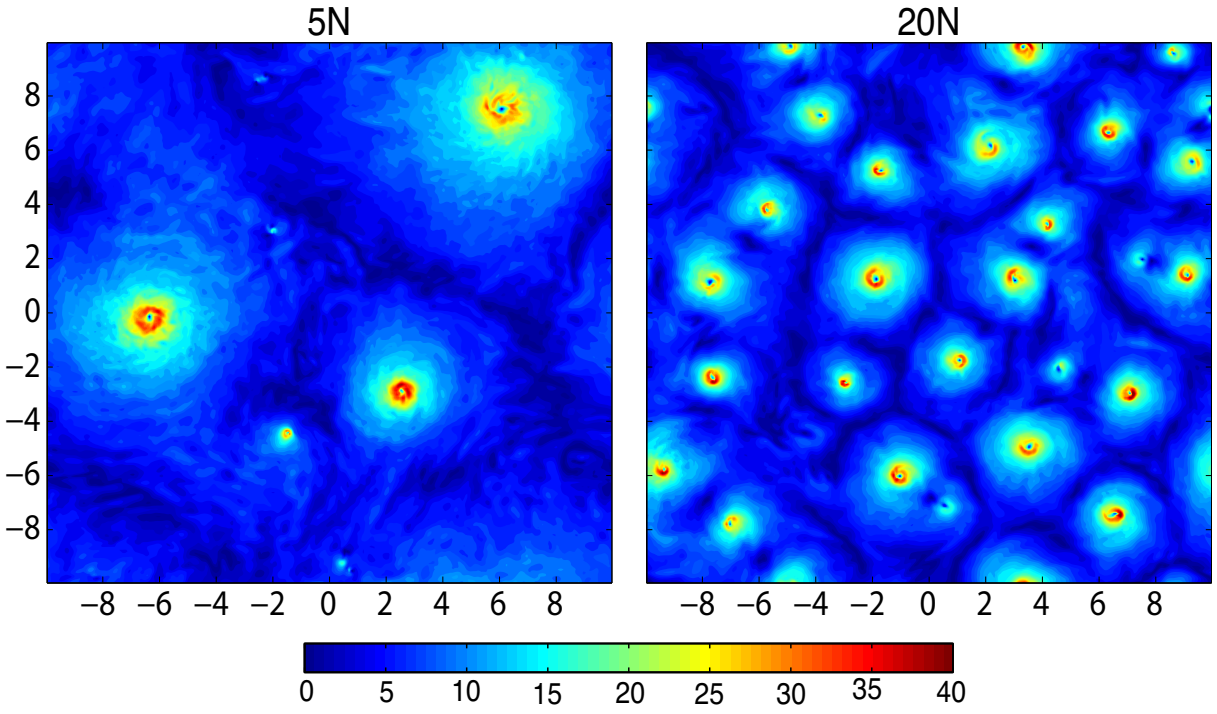

Figure 7. Snapshots of surface wind speed ($\mathrm{m\,s^{-1}}$) for ambient rotation rates corresponding to 5N (left) and 20N (right), in 55 km model with SST = 305K.

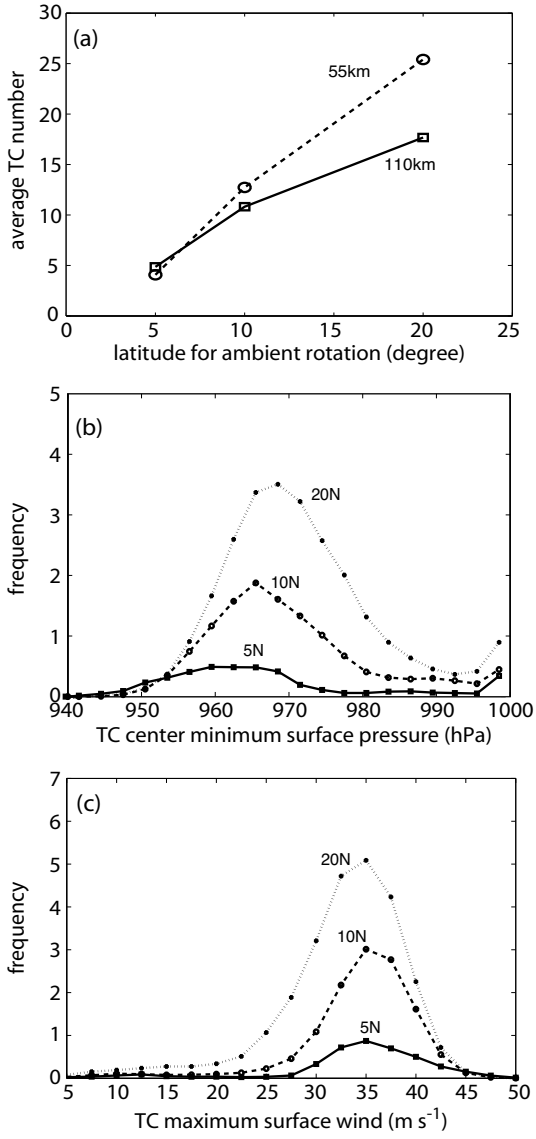

Figure 8. a) Sensitivity of storm number to ambient rotation rate. b) PDF of minimum storm surface pressure as a function of ambient rotation for the 55 km model. c) As in b) but for maximum storm surface wind.